Natural Hazards
https://doi.org/10.1007/s11069-022-05622-2

ORIGINAL PAPER

ARIMA model simulation for total electron content, earthquake and radon relationship identification

Sinan Keskin[1] · **Fatih Külahcı**[1]

Received: 1 October 2021 / Accepted: 15 September 2022

Abstract

Earthquakes cause many losses of life and property with their devastating effects. Scientists conduct studies to predict the hazards by examining the anomalies that occur before the earthquake. In this study, mathematical and statistical relationships are examined between soil radon (Rn-222) gas and earthquake and atmospheric total electron content (TEC). Furthermore, an Autoregressive Integrated Moving Average (ARIMA) simulation model is proposed to predict Rn concentrations. The model is evaluated for the M 4.2 Sivas, Susehri earthquake in Türkiye that took place on the North Anatolian Fault Zone in 2007 and a relationship is determined between soil Rn gas and micro-seismic activity. In parallel with the earthquake–radon relationship, some meteorological variables [5, 10, 20, 50 cm soil temperature (°C), vapour pressure (hPa), wet bulb temperature, dry bulb temperature] are identified as associated with the earthquake. It is also observed that the TEC increases with the relative Rn gas concentration as the time of the main shock is approached. This provides meaningful results for further seismo-ionospheric change interpretations. In addition, the ARIMA model detects possible future Rn gas concentration values.

Graphical abstract

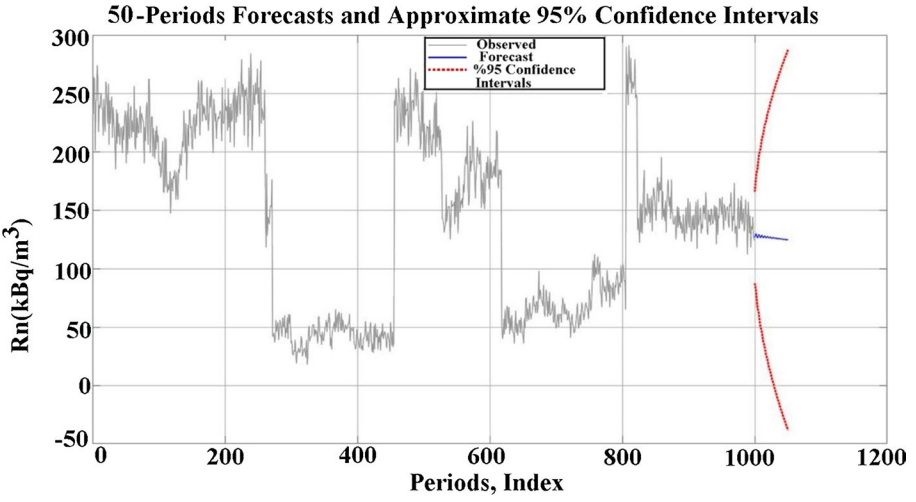

Extended author information available on the last page of the article

Published online: 23 September 2022

Keywords Forecasting simulation · Modelling · Soil radon gas · Risk analysis · Prediction

1 Introduction

Earthquakes caused 2.7 million deaths between 1900 and 1976 (Randall and David 1993). For this reason, earthquake prediction is the scientific activity of researchers working in this field. So far, researchers have proposed many methods and techniques for earthquake predictions in hopes to find a solution (Martin et al. 2016). The rate of P-wave changes, ground slope and elevation, reduction in electrical resistance of rocks, groundwater level fluctuations and oil flow, magnetic fields, ionospheric changes, crustal resistance, landslides, gravitational effects, and radon emissions are used to predict earthquakes performances. Studies on the identification of these earthquake precursors are increasing (Crockett et al. 2006; Külahcı and Şen 2014). This research concentrates on the aforementioned precursors including Rn and ionospheric TEC.

Rn (in article, the word Rn is used for the isotope ^{222}Rn) is produced continuously by the decay of ^{226}Ra in the uranium decay chain and is an inert gas (Kim et al. 2018; Singh et al. 1999; Tanner 1964). Several studies have suggested that due to its short half-life of 3.82 days, ease of detection and atmospheric transport monitoring of Rn concentration in soil as a function of time may be useful for predicting upcoming earthquakes (Ghosh et al. 2009; Wang et al. 2014; Yalım et al. 2012). Rn gas from the depths of the Earth formed under the influence of tectonic stress migrates towards the Earth crust through the ground cracks along the fault zones and is released towards the Earth's surface (Woith 2015). Spatial and temporal patterns of deep source gas seepage are studied by measuring soil gas in active fault zones (Ciotoli et al. 2007; Külahcı and Şen 2014; Kuo et al. 2006).

The interest in anomalies in pre-earthquake Rn concentration started with Okabe's (1956) investigation of the relationship between interactions of the atmospheric Rn values and earthquakes. Ulomov and Mavashev (1971) showed that the Tashkent earthquake affected the radon concentration in groundwater. Many researchers tried to relate radon anomalies in soil and water to seismic activity (Ge et al. 2014; Ghosh et al. 2011; Gregorič et al. 2012; Hauksson 1981; Hauksson and Goddard 1981; Igarashi et al. 1995; Igarashi and Wakita 1990; Imme and Morelli 2012; Khan et al. 1990; King, 1980; Külahcı and Çiçek 2015; Kuo et al. 2006; Kuo and Tsunomori 2014; Mogro-Campero et al. 1980; Nishizawa et al. 1998; Noguchi and Wakita 1977; Singh et al. 1999).

In the second half of the twentieth century, scientists discovered that anomalies in the earthquake preparation process should be sought not only in the lithosphere but also in the ionosphere. The first study was the observation of earthquake-related ionospheric anomalies during the 1964 great Alaska earthquake (Davies and Baker 1965). Antsilevich and Vilenskii (1971) and Datchenko and Ulomov (1972) analysed the observations of the ionospheric vertical sounder, suggesting that the abnormal increase in electron content before the 1966 Tashkent earthquake could be a precursor to the Tashkent earthquake. Afterwards, ionospheric anomalies related to seismic activity aroused wide interest among the researchers and ionospheric TEC as an earthquake precursor (Bhattarai et al. 2018; Hattori et al. 2014; Huang et al. 2017; Kalita et al. 2012; Li and Parrot 2018; Liu et al. 2009; Oikonomou et al. 2016; Perrone et al. 2018; Pulinets et al. 2007; Sergei Pulinets and Boyarchuk 2004; Şentürk and Çepni 2018; Sharma et al. 2017; Ulukavak and Yalçınkaya 2017a; Zhao et al. 2008). TEC is the amount of electrons in a cylinder with a base of 1 m^2 along the line between the receiver and the electromagnetic

signal, largely determined by the maximum electron concentrations of the F2 layer, and its unit is TECU. 1 TECU = 10^{16} electrons/m^2.

Volcanic eruptions, natural ground radioactivity, radioactive pollution, rocket and space shuttle launches, ballistic missiles, asteroids and even surface mine explosions generate significant ionospheric anomalies. Solar (coronal Solar flares and mass outflows), atmospheric (storms and lightning strikes), and meteorological events (typhoons and hurricanes) and earthquakes can cause ionospheric disturbances (Dautermann et al. 2007; Garrison et al. 2007; Gautam et al. 2019; Laakso 2002; Liu et al. 2006; Pulinets and Ouzounov 2011; Schunk and Nagy 2010). Changes in the vertical electric and magnetic fields may occur in the earthquake preparedness zone and its immediate surroundings. As the effect of these movements towards the atmosphere, the total electron content of the ionosphere changes due to the combination of the neutral atmosphere environment and the ionized ionospheric plasma (Sharma et al. 2017). TEC changes in the ionosphere can also be determined by GNSS observations before, during and after the earthquake (Başçiftçi et al. 2018; Zolotov et al. 2012). TEC anomalies can be observed in positive and negative directions before and after earthquake occurrences (Çepni and Şentürk, 2015; Fuying et al. 2011; Liu et al. 2006; Sezen et al. 2013; Shah and Jin 2018; Zolotov et al. 2012).

Pulinets and Boyarchuk (2004) studied the process of strong vertical electric field formation in the earthquake preparedness zone before an earthquake. Radon emanations from the Earth's crust in seismically active regions cause to ionized air (Pulinets and Liu 2004). It is known that intense gas discharges such as CO_2, methane and nitrogen occur mostly from the Earth crust in the preparation zone before the earthquake (Kuo et al. 2013). These gas oscillations generate air movement leading to instabilities that can stimulate acoustic gravitational wave generations. Since the Coulomb force is not very strong, intense air movements disperse the neutral clusters. In a short time, the near-ground layer of the atmosphere becomes enriched with ions (estimated concentration 10^5–10^6 cm^3). The ionization leads to the formation of abnormally strong vertical electric fields compared to the normal air electric field (Liu et al. 2004; Sharma et al. 2017; Kim et al. 2018). Many researchers have conducted studies to explain the cause of these anomalies in TEC. Freund (2007) suggested the P-type semiconductor effect for the cause of the vertical electric and magnetic field in the earthquake preparedness zone. When rocks on the earth are stretched and compressed the peroxy bonds are broken and electrically charged carriers are released to form positive holes, which are very mobile and can be moved easily from the trapped zone to the free zone (Freund, 2000; Lin, 2012; Namgaladze et al. 2018; Ulukavak and Yalcinkaya 2017b).

One of the rapidly developing areas in earthquake forecasting is the ground surface thermal anomaly studies that occur a few days before strong earthquakes in the preparation areas. The time scale of the thermal anomalies formation is very similar to the time scale of ionospheric precursors (Pulinets 2004). A large amount of water vapour molecules (10^{17} cm^3) in the troposphere undergoes hydration quickly with basic ions, and hence, the humidity in the air decreases and as a result of this exothermic event, heat is released to the environment, which causes the temperature to increase in the earthquake preparedness zone. This increase in air temperature leads to variability in air conductivity (Izhovkina et al. 2006; Schekotov et al. 2021).

Sources such as atmospheric or underground explosions and shallow earthquakes cause to strong vertical ground displacements, which are known to produce pressure wave propagations in the atmosphere at infrasonic speeds (Lognonné et al. 2006). Low-frequency acoustic waves are coupled with the gravitational waves in the ionosphere cause variations

in electron density in the region (Fuying et al. 2011; Jin et al. 2011; Liperovsky et al. 2008; Schekotov et al. 2021).

The aim of this study is to evaluate the soil ^{222}Rn gas concentration, TEC variations and earthquakes simultaneously in order to examine the possible mathematical and statistical relationships between them, and hence, to propose an ARIMA model for the relationships. This model helps to determine the ^{222}Rn concentration on the North Anatolian Fault Zone (NAFZ), which is one of the most seismically active fault zones on this side of the Earth. Simultaneous analyses of this triple change of Rn, TEC and earthquakes lead to one step further improvement in earthquake prediction studies. In addition, observation and analysis of meteorological variables [5, 10, 20, and 50 cm soil temperature (°C), vapour pressure (hPa), wet bulb temperature, dry bulb temperature] together with this triple change is an important reference source for relevant researchers.

2 Material and method

2.1 Time series analysis and ARIMA model

A time series is a set of numerical data taken sequentially at equal time intervals within a certain period of time (Fanoodi et al. 2019**). Examples of time series abound in fields such as economics, business, engineering, natural sciences (especially earth sciences, geophysics and meteorology), and social sciences. Adjacent observations in a time series are serially dependent and different techniques are used to analyse this dependency. Among the application areas of time series are the following points.

1. Estimation of the future values by learning from past and current values,
2. Determination of the transfer function of an inertial system through a dynamic input–output model that can show the effect of any input series on the output system,
3. The use of indicator input variables in transfer function models to represent and evaluate the effects of disruptive interventions in a time series,
4. Examination of the relationships between various relevant time series and identification of suitable multivariate dynamic models to represent common relationships between variables over time,
5. Design of simple control schemes in which potential deviations of the system output from a desired target can be compensated as much as possible by the input series values adjustment (Box et al. 2015).

A very powerful time series forecasting tool is ARIMA (Autoregressive Integrated Moving Average) or Automatic Tension Integrated Moving Average approach, which combines three separate parts into a comprehensive model. The first piece is the autoregressive or "AR" term, which corresponds to the number of lagged values of the residuals in the unconditional prediction model. The model captures the historical real data variation into a predictive model and uses variation to build a better predictive model. The second piece is the order of integration or the term "I", which corresponds to the number of differentiations of the time series to render into a stationary structure. This element takes into account possible nonlinear growth rates in the data. The third piece is the term "MA", which is essentially the moving average of the lagged forecast errors (Şen 2009, 2016). The model

essentially learns from forecast errors and corrects them with a moving average calculation by including this component of delayed forecast errors.

ARIMA (p.d.q) models are extensions of the AR model, which uses three components to model serial correlation in time series data. As noted earlier, the first component is the autoregressive AR(p) model, which uses the p delays of the time series in the equation. The second component is the integration (d) term. I(d) means to d fold differentiation. The MA(q) model uses the q delays of the prediction errors to improve the prediction (Akdi 2003; ArunKumar et al. 2021; Box and Jenkins 1976; Hamilton 1994; Roy et al. 2020; Yaffee and McGee 1996).

The ARIMA (p.d.q) model is expressed by the following formula.

$$Y_t = a_1 Y_{t-1} + a_2 Y_{t-2} + \cdots + a_p Y_{t-p} + e_t - b_1 e_{t-1} - b_2 e_{t-2} - \cdots - b_q e_{t-q} \quad (1)$$

The interpretation of the ARIMA model results are almost the same as for multivariate regression analysis. There are several additional sets of results specific to the ARIMA analysis. The first is the addition of Akaike Information Criteria (AIC) and Bayesian Information Criteria (BIC), which are frequently used in ARIMA model selection and description. The AIC and BIC measures are used to determine whether a particular model with a given set of p, d, and q parameters has good statistical fit. While BIC is a defined criterion on the design of the real model, AIC allows the determination of the most suitable model for the data type. The ARIMA model with the lowest BIC and AIC values are the best ones. On the other hand, autocorrelation function (ACF) and partial autocorrelation function (PACF) are the methodologies that are taken into consideration in any ARIMA model validity tests. ACF graphs provide information about the stationarity of the series (Hyndman and Athanasopoulos 2021; Mun 2006; Schaffer et al. 2021; Şen 1992, 2016; Sevüktekin and Çınar 2017; Shumway and Stoffer 2017; Zhang et al. 2014).

3 Research area and data

The research area is Sivas, Susehri (Lat 40.16259 and Long 38.13503) on the North Anatolian Fault Line, Turkey, which has the capacity to produce continuous earthquakes. Soil Rn data over this line are obtained from the Turkish Prime Ministry General Directorate of Disaster Affairs (https://en.afad.gov.tr/). Soil Rn data are measured using Alpha Meter 611 (Alpha Nuclear Co., Canada) detectors. The earthquake data used in the study are obtained from Bogazici University Kandilli Observatory and Earthquake Research Institute Regional Earthquake-Tsunami Monitoring and Evaluation Centre (http://www.koeri.boun.edu.tr/sismo/zeqdb/). The meteorological data as daily and locally; 5, 10, 20 and 50 cm soil temperature (°C), vapour pressure (hPa), wet and dry bulb temperatures are obtained from the Turkish Meteorology General Directorate (https://www.mgm.gov.tr/eng/forecast-cities.aspx). TEC data are obtained from IONOLAB-Ionospheric Research Laboratory (http://www.ionolab.org/index.php?page=index&language=en) (Sezen et al. 2013).

4 Results and discussion

The seismic activity of the research area is extremely high. It is well-known that between 04.07.2007 and 01.24.2010, there were 87 earthquakes with varying magnitudes between 3.1 and 4.2 on the Richter scale. In this study, it is decided to examine the effects of the

Table 1 Earthquakes that occurred between 07/04/2007 and 21/01/2010 in a circle with a diameter of 100 km, the centre of which is Suşehri (Boğaziçi, 2021). Bold values show the two largest earthquakes in the area that occurred on the same day

Date	*D*(km)	*M*	Date	*D*(km)	*M*	Date	*D*(km)	*M*
24.01.2010	8.4	3.4	30.10.2008	5.4	3.3	27.10.2007	7.2	3.1
24.01.2010	15.5	3.1	23.09.2008	8.4	3.1	26.10.2007	7.7	3.3
13.01.2010	4	3.3	17.09.2008	19.3	3.1	15.10.2007	7.5	3.4
19.10.2009	5.5	3.5	01.09.2008	6	3.2	10.10.2007	5.5	3.3
02.10.2009	4.1	3.4	04.08.2008	5.1	3.3	11.09.2007	5.4	3.1
05.09.2009	3.5	3.1	21.07.2008	9.9	3.2	03.09.2007	5	3.7
26.08.2009	8	3.1	25.06.2008	4.9	4	28.08.2007	5	3.3
02.08.2009	10.9	3.1	19.06.2008	3.3	3.1	27.08.2007	3.7	3.5
18.07.2009	2.5	3.2	18.06.2008	5.4	3.2	22.08.2007	2.6	3.2
14.07.2009	2.3	3.2	11.06.2008	5	3.5	17.08.2007	5	3.3
31.05.2009	5.4	3.6	29.05.2008	7.8	3.1	16.08.2007	12.3	3.4
14.05.2009	5	3.1	26.05.2008	9.2	3.2	**06.08.2007**	**6.5**	**3.2**
13.05.2009	2.4	3.4	26.05.2008	4.2	3.2	**06.08.2007**	**5**	**4.2**
21.04.2009	7.7	3.2	20.05.2008	5.5	3.3	03.08.2007	9.2	3.2
19.04.2009	5.4	3.1	16.05.2008	5.4	3.1	01.08.2007	4.1	3.4
27.03.2009	12.3	3.2	27.04.2008	5	3.1	20.06.2007	12.6	3.3
23.03.2009	4.8	3.2	26.04.2008	8.9	3.1	16.06.2007	3.2	3.6
18.03.2009	7.7	3.1	24.04.2008	5.4	3.1	16.06.2007	5	3.6
18.03.2009	7.3	3.3	08.04.2008	5	3.1	15.06.2007	5.3	3.1
17.03.2009	5	3.5	14.02.2008	5	3.3	05.06.2007	12.9	3.2
17.03.2009	3.6	3.4	26.01.2008	5	3.3	14.05.2007	5	3.2
28.02.2009	6.3	3.1	23.01.2008	5	3.4	09.05.2007	6.3	3.1
08.01.2009	13	3.1	23.01.2008	5.3	3.1	08.05.2007	5	3.7
08.01.2009	13.6	3.1	22.01.2008	5	4	08.05.2007	5.3	3.3
07.12.2008	8.6	3.3	29.12.2007	5	4.1	05.05.2007	5.3	3.2
02.12.2008	5.4	3.2	23.12.2007	2.5	3.1	16.04.2007	5.8	3.5
01.12.2008	4.8	3.6	21.12.2007	5.4 3.1		07.04.2007	9.6	3.4
21.11.2008	8.5	3.2	13.12.2007	20.7	3.1			
16.11.2008	5	3.1	04.11.2007	5	3.4			
04.11.2008	3.2	3.6	04.11.2007	2	3.2			

M4.2 (depth 5 km, 06.08.2007) earthquake, which is the largest record in the region, and M3.2 (depth 6.5 km, 06.08.2007) earthquakes on other physical parameters, since it occurred on the same day (Table 1).

The changes in the behaviour of radon with the earthquakes that occurred are given in Fig. 1.

An earthquake with a magnitude of M 3.5 occurred on 04.16.2007 during the first period of Rn data. During this period, it is observed that the Rn gas level in the soil is at the highest levels during the study period. M 4.2 and M 3.2 earthquakes occurred on 06.08.2007 and three earthquakes with M4.1 magnitude occurred on 12.29.2007. After these three relatively large earthquakes, sudden decreases are observed in the radon gas levels in the soil (Crockett et al. 2006; Külahcı and Şen 2014). Smaller earthquakes accompanied the

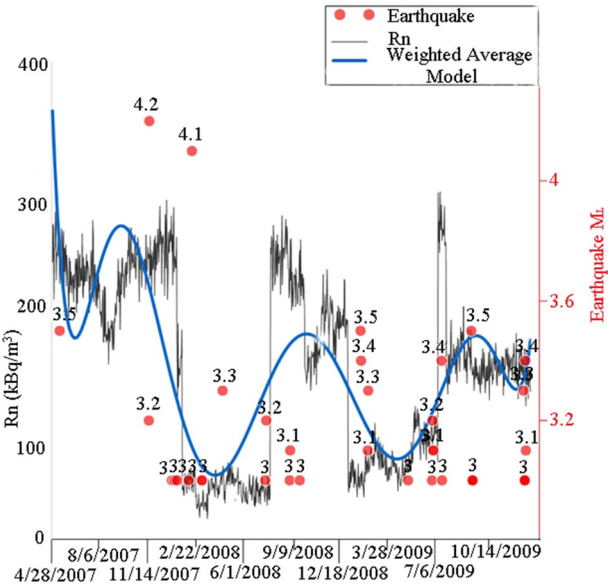

Fig. 1 Radon data and earthquakes

changes in Rn levels after these earthquakes. Considering the time period of the research, it is determined by the Weighted Average Graph that the Rn concentration is in a cyclical filling-discharging period (Fig. 1, Table 1).

Changes in meteorological parameters (5, 10, 20 and 50 cm, soil temperature (°C), vapour pressure (hPa), wet bulb temperature and dry bulb temperature) within the times of the above-mentioned earthquakes also gave statistically significant results. Meteorological parameter data are given in Table 2.

Parallel to the earthquake–radon relationship seen in Figs. 1 and 2 is obtained by making use of Table 2 for the changes of the earthquake with some meteorological variables. It is observed that all meteorological variables started to decrease after the M 4.2 and M 3.2 earthquakes. Especially, after the 4.2 and 4.1 earthquakes, a clear discharge curve appears in the Rn gas concentration. After the discharge, stagnation at the Rn level is observed with chain earthquakes. It took 7 months for Rn gas levels to form a positive peak curve in the research area, which has a permeable soil structure. At the end of this process, it is observed that the previous sinusoidal cycle is repeated with repeated earthquakes. It is seen that this sinusoidal loop explains an Rn-Earthquake characteristic of the region over the measured 2-year period.

TEC data before and after M 4.2 and M 3.2 earthquakes on 08.06.2007 are obtained from Trabzon fixed GPS station, which constantly collects data via IONOLAB group, which provided real-time TEC values with an online calculation system for IGS and/or EUREF stations at www.ionolab.org (Sezen et al. 2013).

Figure 3 shows simultaneous variations of the Ionospheric TEC with earthquake and Rn gas concentration. As the time is approached to the M 4.2 and M 3.2 earthquakes, a noticeable increase is observed in the TEC concentration along with the Rn gas concentration. This shows that Rn can be included in the calculations more effectively about the future of seismo-ionospheric changes.

Table 2 Soil temperature data for August 2007

Day	5 cm soil (°C)	10 cm soil (°C)	20 cm soil (°C)	50 cm soil (°C)	Local vapour pressure (hPa)	Wet thermometer (°C)	Dry thermometer (°C)
1	22.2	24.3	25.4	26.2	14.1	15.0	20.2
2	23.6	24.6	25.6	26.1	15.9	16.0	20.0
3	21.2	23.6	25.2	26.2	16.3	15.0	16.3
4	18.8	22.0	24.4	26.2	13.7	12.4	13.6
5	19.1	21.9	24.2	26.0	14.6	13.2	14.2
6	21.2	23.4	25.0	26.0	14.5	13.8	16.0
7	21.6	23.4	25.0	26.2	14.2	14.6	18.8
8	23.0	25.1	26.2	26.5	19.1	17.6	19.4
9	20.7	23.8	25.4	26.6	17.1	15.7	17.0
10	19.6	23.0	25.2	26.7	15.2	13.8	14.8
11	19.4	23.0	25.2	26.7	13.6	13.0	15.4
12	20.2	23.4	25.3	26.7	14.1	13.9	17.0
13	21.4	24.4	26.0	26.8	11.7	12.6	17.6
14	21.6	24.5	26.3	27.2	17.6	16.3	18.0
15	22.0	24.4	25.8	27.1	16.4	15.4	17.3
16	20.2	23.4	25.6	27.0	15.6	14.5	16.0
17	20.1	22.2	25.3	27.0	17.5	15.6	16.0
18	18.2	20.6	24.2	27.0	15.0	13.4	14.0
19	17.8	21.2	23.6	26.2	14.7	13.1	13.8
20	19.1	22.2	24.2	26.1	16.4	14.6	15.0
21	19.0	21.0	23.9	26.0	13.8	13.0	15.1
22	20.6	23.0	24.6	26.0	15.6	14.8	17.0
23	18.9	22.0	24.2	26.0	16.5	15.0	16.0
24	19.6	21.0	23.6	25.6	15.8	15.0	17.2
25	18.0	21.0	23.2	25.4	15.1	13.8	15.0
26	17.2	20.0	22.2	25.0	15.4	14.0	15.0
27	19.4	21.0	22.4	24.7	17.4	15.6	16.2
28	15.8	18.8	21.4	24.3	13.4	11.6	12.0
29	16.4	19.4	21.8	24.2	15.8	14.4	15.4
30	14.0	16.6	20.0	23.8	14.2	12.6	13.2
31	14.4	17.4	20.6	23.5	12.5	11.2	12.6

4.1 ARIMA model

The MATLAB software is used to obtain an ARIMA model (Şen 2019) for the predictions of the Rn gas over the unmeasured forward time periods. The procedure for finding a suitable model is based on a series of steps (Külahcı 2020), which includes appropriate transformation and differentiation, detection of the ARIMA model, estimation of parameters, and diagnostic control of residues through Ljung-Box statistics (Box et al. 2015).

The time-dependent variation of Rn is given in Fig. 4, and the autocorrelation and PACF graphs are in Fig. 5a, b using Rn data. In a series with a trend effect, the autocorrelation

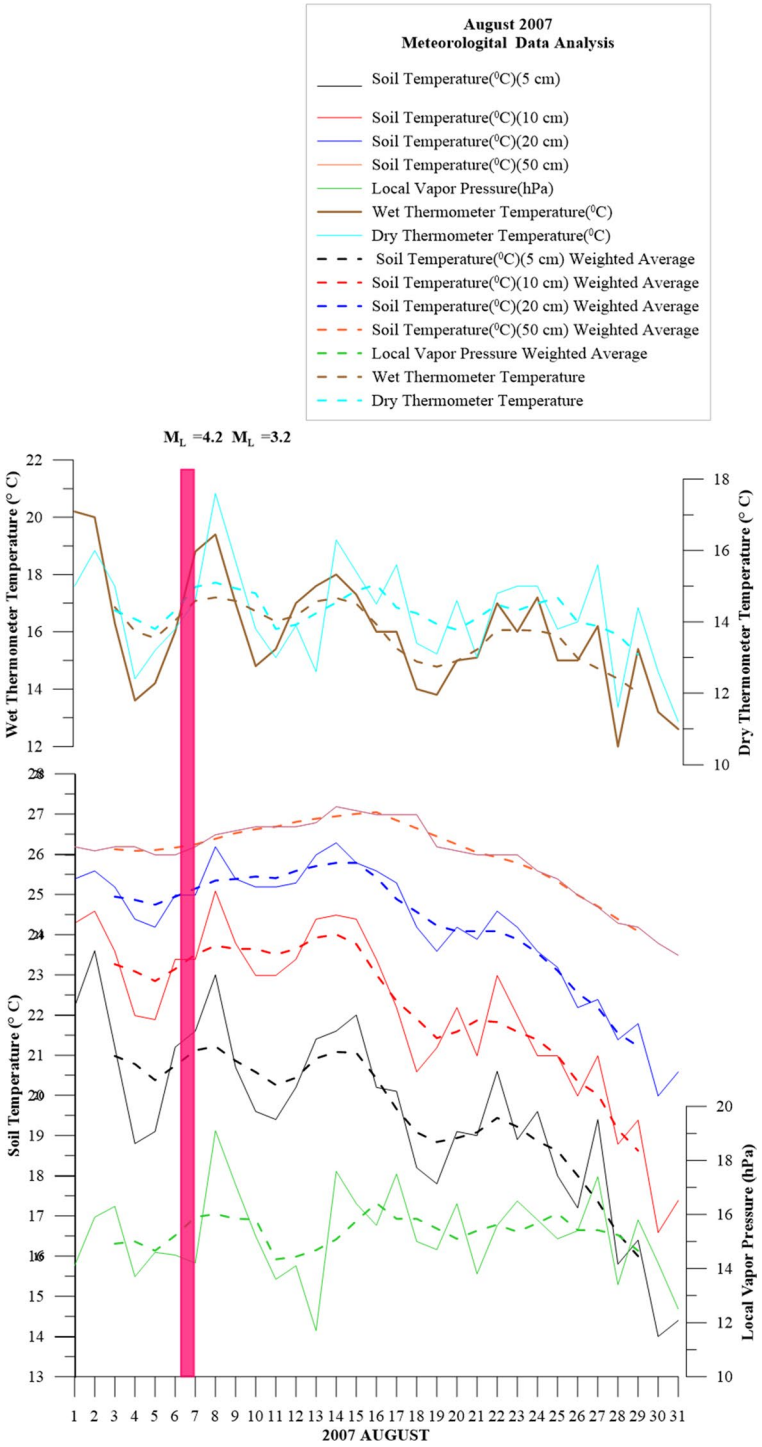

Fig. 2 Meteorological change parameters of August 2007, when the earthquake occurred

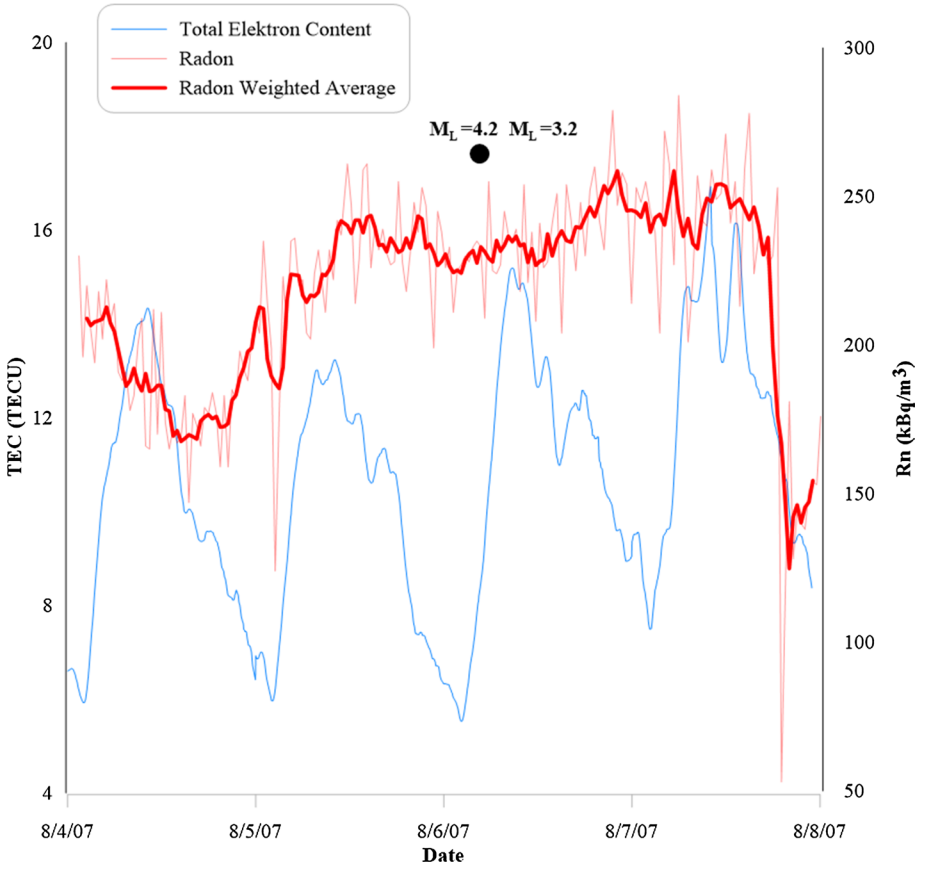

Fig. 3 TEC, radon and earthquake graph before and after the M 4.2 and M 3.2 earthquakes on 08/06/2007

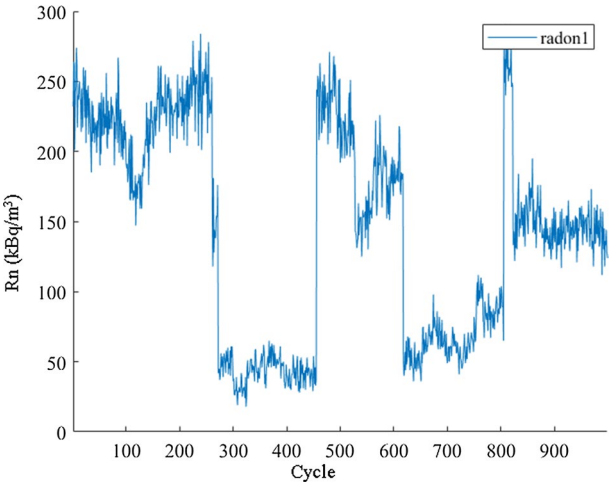

Fig. 4 Time series graph of radon values

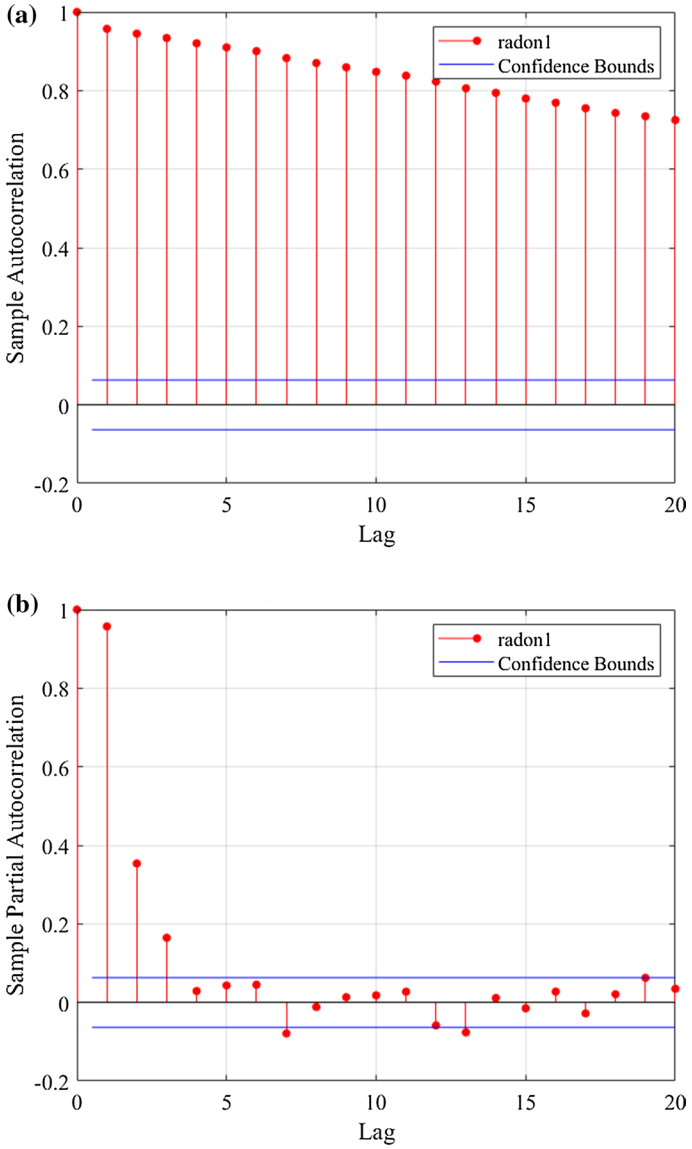

Fig. 5 **a** Autocorrelation function graph of Rn data, **b** partial autocorrelation function graph of Rn data

function appears as positive and high for short lags with slow decrease as the lag increases. If the autocorrelations do not decrease or disappear rapidly, the series is non-stationary (ArunKumar et al. 2021). In this case, the difference of the data is taken until stationarity is achieved and then, an ARIMA model is matched. From the Rn values in Fig. 5a, it is understood that the series is not stationary. The graph of Rn after taking the difference of the series is given in Fig. 6, while the graphs of ACF and PACF are presented in Figs. 7a and b. In addition, histogram of residual values and distribution-scatter (Q–Q) graph of residual values are given in Fig. 8a and b.

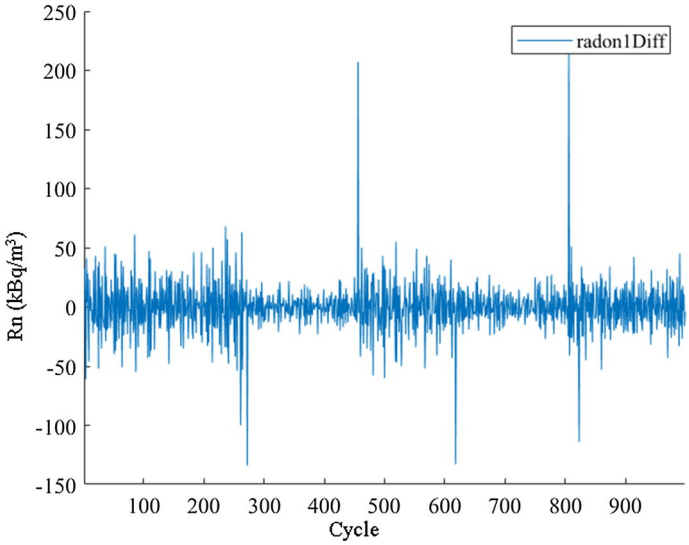

Fig. 6 The change of Rn data after taking the difference

For statistical control of the stationarity, the Augmented Dickey-Fuller Test (ADF) is performed (Cheung and La1995; Sevüktekin and Çınar 2017). ADF test results are given in Tables 3 and 4.

If the value of the test statistic is less than the critical value, it is understood that the series is stationary (Tortum et al. 2014). According to the ADF test results, the Rn time series is now stationary. The ACF and PACF graphs of the differentiated series give useful information about the AR and MA values. In the ACF and PACF graphs show downward trend to the confidence band then the number of delays provides information about the approximate MA and AR values, respectively, and accordingly, MA = 1 in the ACF graph and AR = 2 in the PACF graph (Akdi 2003; Mun 2006). Since graphical analysis yields information to some extent, performing additional statistical analyses give the most reliable and accurate result. It is, therefore, necessary to obtain AIC and BIC values for each ARIMA model. From Table 5 it is possible to understand that many ARIMA models are the best that explain the data at hand. The most suitable ARIMA model is ARIMA (4.1.3) as can be seen from the smallest AIC and BIC values (Table 5).

The equation according to the Rn time series is suitable for the model according to the following equation and the normal (Gaussian) probability distribution function.

$$(1 - \phi_1 L - \cdots - \phi_4 L^4)(1 - L)y_t = c + (1 + \phi_1 L + \phi_2 L^2 + \phi_3 L^3)\varepsilon_t \tag{2}$$

The details of the results are obtained by entering the Rn data into the model and the results are presented in Tables 6 and 7.

One can use the ARIMA (4.1.3) model as a simulation application for Rn forward timeframes (the next 50 steps with unknown value) (Külahcı 2020). The prediction of radon data can be obtained from the simulation study using ARIMA (4.1.3) as given in Fig. 9. The portion between the curves indicated by the red confidence (95%) lines is the arithmetic mean of the estimated Rn values. Figure 10 is an enlarged representation of this mean.

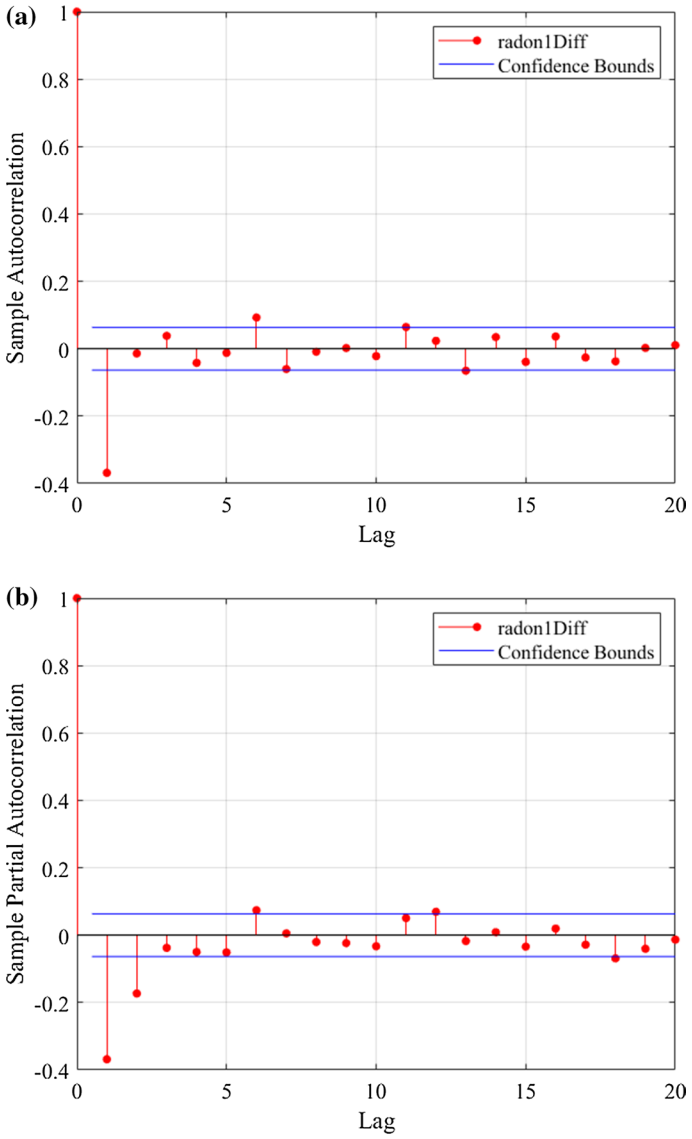

Fig. 7 **a** Autocorrelation function graph of the differenced series, **b** partial autocorrelation function graph of the differenced series

5 Conclusions

The large number of earthquakes that occurred in the North Anatolian Fault Zone (NAFZ) at the time of the radon data records is one of the proofs that this region is one of the most seismically active continental strike-slip fault zones in the world. The impact of earthquakes significantly affects radon concentrations. In the earthquake

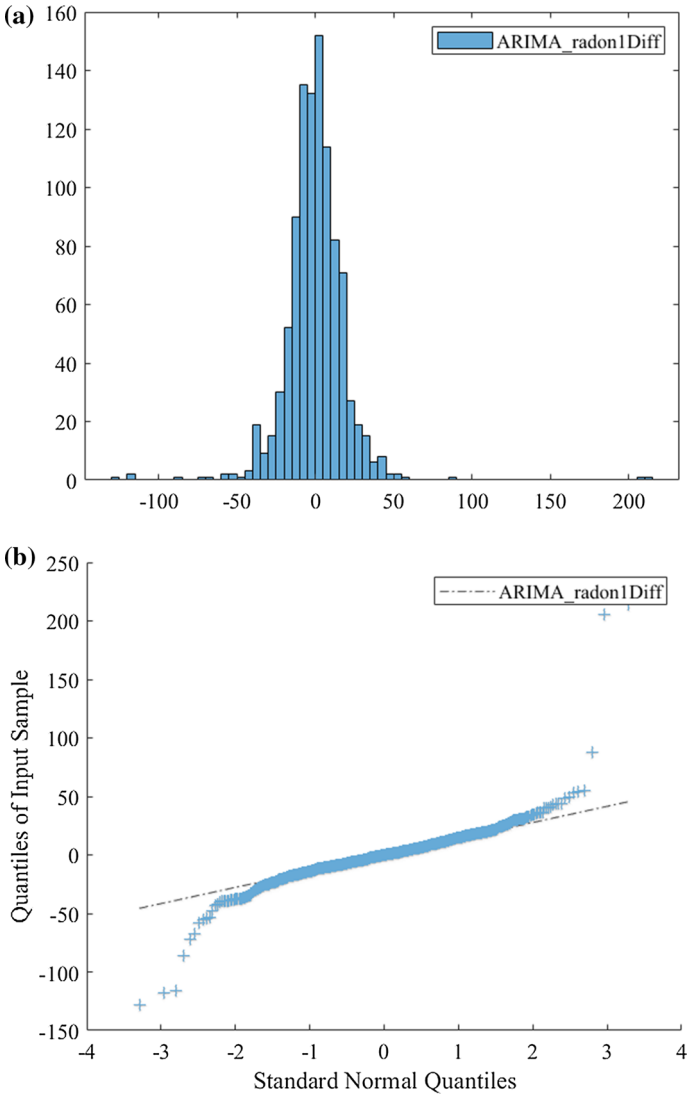

Fig. 8 **a** Histogram chart of residual values, **b** distribution–distribution (Q-Q) chart of residual values

Table 3 Test parameters

	Lags	Model	Test statistics	Sig level
1	0	AR	t1	0.05

Table 4 Test results

	Null rejected	*P*-Value	Test statistic	Critic value
1	True	0.001	−46.4791	−1.9416

Table 5 AIC and BIC values of the recommended models

Model	AIC–BIC		Model	AIC–BIC	
ARIMA (1.1.0)	AIC	9512.432	ARIMA (4.1.4)	AIC	8844.1094
	BIC	9527.143		BIC	8893.1167
ARIMA (1.1.1)	AIC	8921.691	ARIMA (5.1.1)	AIC	8867.2963
	BIC	8941.305		BIC	8906.494
ARIMA (1.1.2)	AIC	8915.481	ARIMA (5.1.2)	AIC	8840.4534
	BIC	8939.999		BIC	8884.5509
ARIMA (1.1.3)	AIC	8882.894	ARIMA (5.1.3)	AIC	8839.3029
	BIC	8912.316		BIC	8888.3002
ARIMA (1.1.4)	AIC	8884.867	ARIMA (5.1.4)	AIC	8829.827
	BIC	8919.194		BIC	8883.726
ARIMA (2.1.1)	AIC	8862.073	ARIMA (6.1.1)	AIC	8866.383
	BIC	8886.586		BIC	8910.472
ARIMA (2.1.2)	AIC	8848.719	ARIMA (6.1.2)	AIC	8842.207
	BIC	8878.136		BIC	8891.194
ARIMA (2.1.3)	AIC	8850.713	ARIMA (6.1.3)	AIC	8829.826
	BIC	8885.032		BIC	8883.712
ARIMA (3.1.0)	AIC	9158.346	ARIMA (6.1.4)	AIC	8858.937
	BIC	9182.855		BIC	8917.722
ARIMA (3.1.1)	AIC	8863.771	ARIMA (6.1.5)	AIC	8845.377
	BIC	8893.182		BIC	8909.067
ARIMA (3.1.2)	AIC	8843.425	ARIMA (6.1.6)	AIC	8868.952
	BIC	8877.737		BIC	8937.534
ARIMA (3.1.3)	AIC	8864.994	ARIMA (7.1.1)	AIC	8865.092
	BIC	8904.207		BIC	8914.069
ARIMA (3.1.4)	AIC	8842.536	ARIMA (7.1.2)	AIC	8843.078
	BIC	8886.652		BIC	8896.953
ARIMA (4.1.1)	AIC	8865.307	ARIMA (7.1.3)	AIC	8831.038
	BIC	8899.613		BIC	8889.811
ARIMA (4.1.2)	AIC	8890.977	ARIMA (7.1.4)	AIC	8846.991
	BIC	8930.184		BIC	8910.661
ARIMA (4.1.3)	AIC	**8826.122**	ARIMA (7.1.5)	AIC	8850.489
	BIC	**8870.228**		BIC	8919.058

Table 6 Model estimation results

Parameter	Value	Standard error	*T* Statistics	Probability value
Constant	0.0009487	0.003199	0.296	0.76682
AR{1}	0.10423	0.057451	1.814	0.069646
AR{2}	−0.78001	0.020698	−37.686	8.5444e−311
AR{3}	−0.32107	0.02257	−14.226	6.359e−46
AR{4}	−0.18718	0.020319	−9.213	3.1922e−20
MA{1}	−1.5514	0.056759	−27.334	1.7001e−164
MA{2}	1.4015	0.077257	18.141	1.5122e−73
MA{3}	−0.85009	0.035472	−23.965	6.4223e−127
Variance	398.575	6.969	57.190	0

Table 7 AIC and BIC values for the model

AIC	8826.122
BIC	8870.28

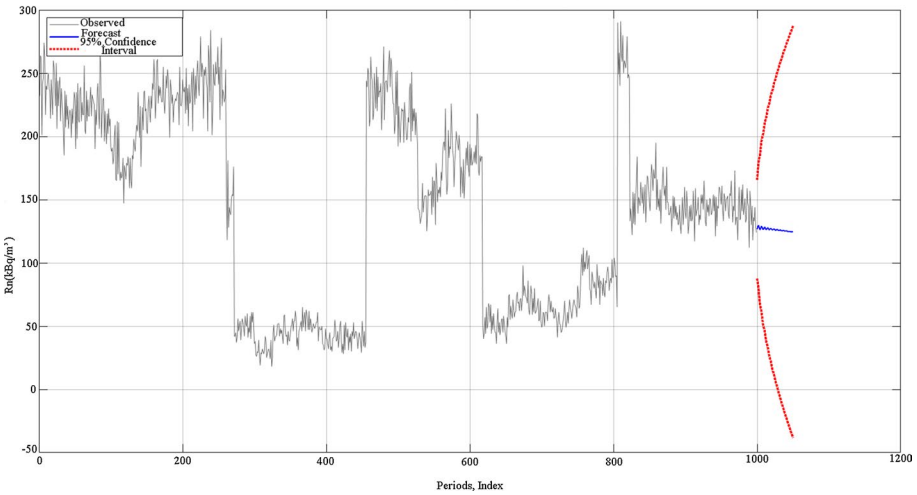

Fig. 9 Simulation giving an estimate of Radon concentrations after 50 steps for unknown time periods

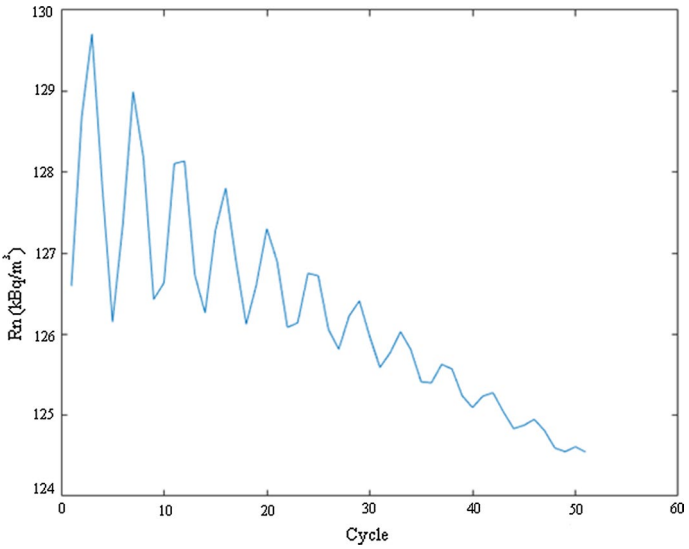

Fig. 10 Variation of 50 simulation steps generated by ARIMA (4.1.3) of the Rn time series for unknown times. The details of the change in the forecast graph given in Fig. 9 can be seen

preparedness zone, radon levels increase with the effect of compression and stress in the rocks and after the earthquake occurrence these values decrease to their normal limits.

Radon fills up cyclically to major earthquakes; it exhibits a discharge period with earthquakes and aftershocks. Regular monitoring of the change in radon levels can give the news of an earthquake approach. In order to make, a rational radon prediction by using time series analysis, the stochastic procedures like the ARIMA (p,q,d) for change in radon levels. In addition, with the establishment of more observation stations, predictions become more reliable by obtaining a large database.

Rn gas emanating from the earth's crust in seismically active regions causes the air to become ionized. The large amount of water vapour molecules in the troposphere hydrates very quickly with the basic ions, and as a result, the humidity in the air decreases and as a result of exothermic event heat is released to the environment. This causes the temperature to increase in the earthquake preparedness zone. One of the rapidly developing research areas of earthquake precursors is the study of ground surface thermal anomalies that occur a few days before strong earthquakes in the preparedness area. The time scale of thermal anomalies formations is very similar to the scale of ionospheric precursor formation. Rn gas emission depends on environmental variables as well as on geological activities. These variables are soil moisture, precipitation, temperature, barometric pressure, wind and tidal forces. The effects of these factors on the transport values of ^{222}Rn in the soil are quite high. It is seen that the soil temperature increased before the M 4.2 earthquakes and the M 3.2 earthquakes that took place on the same day, and decreased after the earthquake. The use of such anomalies as a predictor of an upcoming earthquake in potential research regions, apart from seasonal and seasonal increases, can be considered as a subject of different studies. In addition, a sinusoidal increase and decrease in amplitude is observed simultaneously with earthquakes for 2 years in the research area. The weighted average of the data provided a clear view of the Rn-Earthquake relationship.

According to the proposed ARIMA simulation, a decrease in Rn gas concentration is observed. The conclusion to be drawn from this may be a pre-estimate earthquake occurrence and the gas descend to normal levels.

The variation of the Ionospheric TEC with earthquake and radon gas concentration is investigated simultaneously, and the simulation of the Rn variable for unknown times is the most important result of this research. In addition, when the main earthquake shocks are approached temporally in the research area, an increase is observed in the TEC concentration along with the Rn concentration. This result is important for future studies on seismo-ionospheric changes.

Acknowledgements Soil Rn data were obtained from the Turkish Prime Ministry General Directorate of Disaster Affairs (https://en.afad.gov.tr/). The earthquake data used in the study were obtained from Boğaziçi University Kandilli Observatory and Earthquake Research Institute Regional Earthquake-Tsunami Monitoring and Evaluation Centre (http://www.koeri.boun.edu.tr/sismo/zeqdb/). Meteorological data (5, 10, 20, and 50 cm soil temperature (℃), vapour pressure (hPa), wet and dry bulb temperatures) we used in our research were obtained from the Turkish Meteorology General Directorate (https://www.mgm.gov.tr/eng/forecast-cities.aspx). TEC data is taken from IONOLAB-Ionospheric Research Laboratory (http://www.ionolab.org/index.php?page=index&language=en). Finally, we would like to thank the referees and especially Editor Prof. Dr. Thomas Glade for his extraordinary management and patience.

Declaration

Conflict of interest We wish to confirm that there are no known conflicts of interest associated with this publication and there has been no significant financial support for this work that could have influenced its outcome. We confirm that the manuscript has been read and approved by all named authors and that there

are no other persons who satisfied the criteria for authorship but are not listed. We further confirm that the order of authors listed in the manuscript has been approved by all of us. We confirm that we have given due consideration to the protection of intellectual property associated with this work and that there are no impediments to publication, including the timing of publication, with respect to intellectual property. In so doing we confirm that we have followed the regulations of our institutions concerning intellectual property.

References

Akdi Y (2003) Zaman Serileri Analizi, Birim Kökler ve Kointegrasyon (pp. 47–112). Bıçaklar Kitabevi, Ankara.

Antsilevich M, Vilenskiy I, Gerasimov G, Grishkevich L, Yelizar'yev Y, Karpenko A, Kolokolov L, Levin M, Leshchenko L, Ovezgel'Dyyev O, Samorokin N, Sukhodol'Skaya A (1971) Effect of the September 22, 1968, Solar Eclipse in the F2-Layer. Geomagnet Aeron 11:458

ArunKumar KE, Kalaga DV, Sai Kumar CM, Chilkoor G, Kawaji M, Brenza TM (2021) Forecasting the dynamics of cumulative COVID-19 cases (confirmed, recovered and deaths) for top-16 countries using statistical machine learning models: Auto-Regressive Integrated Moving Average (ARIMA) and Seasonal Auto-Regressive Integrated Moving Averag. Appl Soft Compu 103:107161. https://doi.org/10.1016/j.asoc.2021.107161

Başçiftçi F, İnal C, Yıldırımm O, Bülbül S (2018) Comparison Of Regional And Global TEC Values: Turkey Model. Int J Eng Geosci 3(2):61–72. https://doi.org/10.26833/ijeg.382604

Bhattarai N, Chapagain NP, Adhikari B (2018) Total electron content and electron density profile observations during geomagnetic storms using COSMIC satellite data. 52(250):1979–1990. arXiv. http://omniweb.gsfc.nasa.gov/ow.html.

Boğaziçi Ü (2021) B.Ü. Kandilli Rasathanesi BDTİM Deprem Sorgulama Sistemi. In: Boğaziçi Üniversitesi Kandilli Rasathanesi ve Deprem Araştırma Enstitüsü Bölgesel Deprem-Tsunami İzleme ve Değerlendirme Merkezi. http://www.koeri.boun.edu.tr/sismo/zeqdb/

Box GEP, Jenkins GM (1976) Time series analysis: Forecasting and control. Holden-Day, San Francisco

Box G, Jenkins G, Reinsel G, Ljung G (2015) Time series analysis: forecasting and control. Wiley, New York

Çepni M, Şentürk E (2015) İyonosferik Değişim ve Deprem İlişkisi Üzerine Bir Deneme: Van Depremi Örneği. 5. Uluslararası Deprem Sempozyumu, 603–611.

Cheung YW, La KS (1995) Lag order and critical values of the augmented dickey-fuller test. J Bus Econ Stat 13(3):277–280. https://doi.org/10.1080/07350015.1995.10524601

Ciotoli G, Lombardi S, Annunziatellis A (2007) Geostatistical analysis of soil gas data in a high seismic intermontane basin: Fucino Plain, central Italy. J Geophys ResSolid Earth 112(5):5407. https://doi.org/10.1029/2005JB004044

Crockett RGM, Gillmore GK, Phillips PS, Denman AR, Groves-Kirkby CJ (2006) Radon anomalies preceding earthquakes which occurred in the UK, in summer and autumn 2002. Sci Total Environ 364(1–3):138–148. https://doi.org/10.1016/j.scitotenv.2005.08.003

Datchenko EA, Ulomov VI (1972) Anomalies in the electron density of the ionosphere as a possible forerunner of a Tashkent earthquake. Institute of Seismology, Tashkent.

Dautermann T, Calais E, Haase J, Garrison J (2007) Investigation of ionospheric electron content variations before earthquakes in southern California, 2003–2004. J Geophys Res Solid Earth 112(2). https://doi.org/10.1029/2006JB004447

Davies K, Baker DM (1965) Ionospheric effects observed around the time of the Alaskan earthquake of March 28, 1964. J Geophys Res 70(9):2251–2253. https://doi.org/10.1029/jz070i009p02251

Freund F (2000) Time-resolved study of charge generation and propagation in igneous rocks. J Geophys Res Solid Earth 105(B5):11001–11019. https://doi.org/10.1029/1999jb900423

Freund FT (2007) Pre-earthquake signals—Part II: Flow of battery currents in the crust. Nat Hazards Earth Syst Sci 7(5):543–548. https://doi.org/10.5194/nhess-7-543-2007

Fuying Z, Yun W, Yiyan Z, Jian L (2011) A statistical investigation of pre-earthquake ionospheric TEC anomalies. Geodesy Geodyn 2(1):61–65. https://doi.org/10.3724/sp.j.1246.2011.00061

Garrison JL, Lee S-CG, Haase JS, Calais E (2007) A method for detecting ionospheric disturbances and estimating their propagation speed and direction using a large GPS network. Radio Sci 42(6). https://doi.org/10.1029/2007RS003657

Gautam PK, Chauhan V, Sathyaseelan R, Kumar N, Pappachen JP (2019) NRIAG Journal of Astronomy and Geophysics Co-seismic ionospheric GPS-TEC disturbances from different source characteristic earthquakes in the Himalaya and the adjoining regions Co-seismic ionospheric GPS-TEC disturbances

from different source characterist. NRIAG J Astron Geophys 7(2):237–246. https://doi.org/10.1016/j.nrjag.2018.05.009
Ge L, Zhao J, Luo Y (2014) The research on earthquake radon anomalies. J Geosci Environ Protect 2(5):38–40. https://doi.org/10.4236/gep.2014.25006
Ghosh D, Deb A, Sengupta R (2009) Anomalous radon emission as precursor of earthquake. J Appl Geophys 69(2):67–81. https://doi.org/10.1016/j.jappgeo.2009.06.001
Ghosh D, Deb A, Sengupta R, Bera S, Sahoo SR, Haldar S, Patra KK (2011) Comparative study of seismic surveillance on radon in active and non-active tectonic zone of West Bengal. India *Radiation Meas* 46(3):365–370. https://doi.org/10.1016/j.radmeas.2010.07.016
Gregorič A, Zmazek B, Džeroski S, Torkar D, Vaupotič J (2012) Radon as an earthquake precursor - methods for detecting anomalies. In S. D'Amico (Ed.), Earthquake Res Anal. IntechOpen. https://doi.org/10.5772/29108
Hamilton J (1994) Time series analysis, 1st edn. Princeton Universty Press, New Jersey, pp. 43–72.
Hattori K, Hirooka S, Kunimitsu M, Ichikawa T, Han P (2014) Ionospheric anomaly as an earthquake precursor: Case and statistical studies during 1998–2013; 2012 around Japan. 2014 XXXIth URSI General Assembly and Scientific Symposium (URSI GASS), 1. https://doi.org/10.1109/ursigass.2014.6929866
Hauksson E (1981) Radon content of groundwater as an earthquake precursor: evaluation of worldwide data and physical basis. J Geophys Res 86(B10):9397–9410. https://doi.org/10.1029/JB086iB10p09397
Hauksson E, Goddard JG (1981) Radon earthquake precursor studies in Iceland. J Geophys Res 86(B8):7037–7054. https://doi.org/10.1029/JB086iB08p07037
Huang F, Li M, Ma Y, Han Y, Tian L, Yan W, Li X (2017) Studies on earthquake precursors in China: A review for recent 50 years. Geodesy Geodyn 8(1):1–12. https://doi.org/10.1016/j.geog.2016.12.002
Hyndman RJ, Athanasopoulos G (2021) Forecasting: principles and practice, 2rd edn. Monash University, Australia. https://otexts.com/fpp3/index.html
Igarashi G, Saeki S, Takahata N, Sumikawa K, Tasaka S, Sasaki Y, Takahashi M, Sano Y (1995) Groundwater radon anomaly before the kobe earthquake in Japan. Science 269(5220):60–61. https://doi.org/10.1126/science.269.5220.60
Igarashi G, Wakita H (1990) Groundwater radon anomalies associated with earthquakes. Tectonophysics 180(2–4):237–254. https://doi.org/10.1016/0040-1951(90)90311-U
Imme G, Morelli D (2012) Radon as earthquake precursor. In: Sebastiano D'Amico (ed) Earthquake research and analysis - statistical studies, observations and planning (pp. 143–160). InTech. https://doi.org/10.5772/29917
Izhovkina NI, Prutensky IS, Pulinets SA, Klos Z, Rothkaehl H (2006) Plasma wave radiation in the main ionospheric trough in the region of the terminator from the APEX satellite data. Geomagnet Aeron 46(6):717–723. https://doi.org/10.1134/S0016793206060065
Jin S, Han L, Cho J (2011) Lower atmospheric anomalies following the 2008 Wenchuan Earthquake observed by GPS measurements. J Atmos Solar-Terrestrial Phys 73(7–8):810–814. https://doi.org/10.1016/j.jastp.2011.01.023
Kalita S, Devi M, Barbara KA, Talukdar P (2012) Soft Computing Technique for Recognition of Earthquake Precursor from Low Latitude Total Electron Content (TEC) Profiles. International Journal of Computer Applications 44(17):11–14. https://doi.org/10.5120/6354-8775
Khan HA, Tufail M, Qureshi AA (1990) Radon signals for earthquake prediction and geological prospection. J Islamic Acad Sci 3(3):229–231.
Kim JW, Joo HY, Kim R, Moon JH (2018) Investigation of the relationship between earthquakes and indoor radon concentrations at a building in Gyeongju, Korea. Nuclear Eng Technol 50(3):512–518. https://doi.org/10.1016/j.net.2017.12.010
King CY (1980) Episodic radon changes in subsurface soil gas along active faults and possible relation to earthquakes. J Geophys Res 85(B6):3065–3078. https://doi.org/10.1029/JB085iB06p03065
Külahcı F (2020) Environmental distribution and modelling of radioactive lead (210): a Monte Carlo simulation application. 15–32. https://doi.org/10.1007/978-3-030-21638-2_2
Külahcı F, Çiçek Ş (2015) Time-series analysis of water and soil radon anomalies to identify micro–macro-earthquakes. Arab J Geosci 8(7):5239–5246. https://doi.org/10.1007/s12517-014-1513-9
Külahcı F, Şen Z (2014) On the correction of spatial and statistical uncertainties in systematic measurements of ^{222}Rn for earthquake prediction. Surv Geophys 35(2):449–478. https://doi.org/10.1007/s10712-013-9273-8
Kuo T, Fan K, Kuochen H, Han Y, Chu H, Lee Y (2006) Anomalous decrease in groundwater radon before the Taiwan M6.8 Chengkung earthquake. J Environ Radioactivity 88(1):101–106. https://doi.org/10.1016/j.jenvrad.2006.01.005

Kuo T, Liu C, Su C, Chang C, Chen W, Chen Y, Lin C, Kuochen H, Hsu Y, Lin Y, Huang Y, Lin H (2013) Concurrent concentration declines in groundwater-dissolved radon, methane and ethane precursory to 2011 M_W 5.0 Chimei earthquake. Radiation Meas 58:121–127. https://doi.org/10.1016/j.radmeas.2013.04.006

Kuo T, Tsunomori F (2014) Estimation of fracture porosity using radon as a tracer. J Petrol Sci Eng 122:700–704. https://doi.org/10.1016/j.petrol.2014.09.012

Laakso H (2002) Earth's ionosphere and magnetosphere: Vol. SP-514 (European Space Agency (ed.); pp. 41–50). ESA Space Science Department. https://ui.adsabs.harvard.edu/abs/2002ESASP.514...41L/abstract

Li M, Parrot M (2018) Statistical analysis of the ionospheric ion density recorded by DEMETER in the epicenter areas of earthquakes as well as in their magnetically conjugate point areas. Adv Space Res 61(3):974–984. https://doi.org/10.1016/j.asr.2017.10.047

Lin JW (2012) Potential reasons for ionospheric anomalies immediately prior to China's Wenchuan earthquake on 12 May 2008 detected by nonlinear principal component analysis. Int J Appl Earth Observ Geoinform 14(1):178–191. https://doi.org/10.1016/j.jag.2011.09.011

Liperovsky VA, Meister CV, Liperovskaya EV, Bogdanov VV (2008) On the generation of electric field and infrared radiation in aerosol clouds due to radon emanation in the atmosphere before earthquakes. Nat Hazards Earth Syst Sci 8(5):1199–1205. https://doi.org/10.5194/nhess-8-1199-2008

Liu JY, Chen YI, Chen CH, Liu CY, Chen CY, Nishihashi M, Li JZ, Xia YQ, Oyama KI, Hattori K, Lin CH (2009) Seismoionospheric GPS total electron content anomalies observed. before the 12 May 2008 M_w 7.9 Wenchuan earthquake. J Geophys Res Space Phys 114(4). https://doi.org/10.1029/2008JA013698

Liu JY, Chen YI, Chuo YJ, Chen CS (2006) A statistical investigation of preearthquake ionospheric anomaly. J Geophys Res: Space Phys 111(5). https://doi.org/10.1029/2005JA011333

Liu JY, Chuo YJ, Shan SJ, Tsai YB, Chen YI, Pulinets SA, Yu SB (2004) Pre-earthquake ionospheric anomalies registered by continuous GPS TEC measurements. Ann Geophys 22(5):1585–1593. https://doi.org/10.5194/angeo-22-1585-2004

Lognonné P, Artru J, Garcia R, Crespon F, Ducic V, Jeansou E, Occhipinti G, Helbert J, Moreaux G, Godet PE (2006) Ground-based GPS imaging of ionospheric post-seismic signal. Planet Space Sci 54(5):528–540. https://doi.org/10.1016/j.pss.2005.10.021

Martin PM, Schorlemmer D, Page M et al (2016) The earthquake-source ınversion validation (SIV) project. *Seismol Res* Lett 87(3):690–708. https://doi.org/10.1785/0220150231

Mogro-Campero A, Fleischer RL, Likes RS (1980) Changes in subsurface radon concentration associated with earthquakes. J Geophys Res 85(B6):3053–3057. https://doi.org/10.1029/JB085iB06p03053

Mun J (2006) Modeling risk: applying monte carlo simulation, real options analysis, forecasting, and optimization techniques. Wiley, New York, pp 261–296

Namgaladze A, Karpov M, Knyazeva M (2018) Aerosols and seismo-ionosphere coupling: aa review. J Atmospheric Solar-Terrestrial Phys 171:83–93. https://doi.org/10.1016/j.jastp.2018.01.014

Nishizawa S, Igarashi G, Sano Y, Shoto E, Tasaka S, Sasaki Y (1998) Radon, Cl- and SO42- anomalies in hot spring water associated with the 1995 earthquake swarm off the east coast of the Izu Peninsula, central Japan. Appl Geochem 13(1):89–94. https://doi.org/10.1016/S0883-2927(97)00058-9

Noguchi M, Wakita H (1977) Method for continuous measurement of radon in groundwater for earthquake prediction. J Geophys Res 82(8):1353–1357

Oikonomou C, Haralambous H, Muslim B (2016) Investigation of ionospheric TEC precursors related to the M7.8 Nepal and M8.3 Chile earthquakes in 2015 based on spectral and statistical analysis. Nat Hazards 83(S1):97–116. https://doi.org/10.1007/s11069-016-2409-7

Okabe S (1956) Time variation of atmospheric radon content near the ground surface with relation to some geophsical phenomenon. Mem Sci Coll Univ Kyoto Ser A28:99–115

Perrone L, De Santis A, Abbattista C, Alfonsi L, Amoruso L, Carbone M, Cesaroni C, Cianchini G, De Franceschi G, De Santis A, Di Giovambattista R, Marchetti D, Pavòn-Carrasco FJ, Piscini A, Spogli L, Santoro F (2018) Ionospheric anomalies detected by ionosonde and possibly related to crustal earthquakes in Greece. Ann Geophys 36(2):361–371. https://doi.org/10.5194/angeo-36-361-2018

Pulinets SA, Kotsarenko AN, Ciraolo L, Pulinets IA (2007) Special case of ionospheric day-to-day variability associated with earthquake preparation. Adv Space Res 39(5):970–977. https://doi.org/10.1016/j.asr.2006.04.032

Pulinets SA, Liu JY (2004) Ionospheric variability unrelated to solar and geomagnetic activity. Adv Space Res 34(9):1926–1933. https://doi.org/10.1016/j.asr.2004.06.014

Pulinets S, Ouzounov D (2011) Lithosphere-Atmosphere-Ionosphere Coupling (LAIC) model - An unified concept for earthquake precursors validation. J Asian Earth Sci 41(4–5):371–382. https://doi.org/10.1016/j.jseaes.2010.03.005

Pulinets Sergei, Boyarchuk K (2004) The basic components of seismo-ionospheric coupling. in: ionospheric precursors of earthquakes. In: The basic components of seismo-ionospheric coupling. In: Ionospheric precursors of earthquakes (pp. 1–47). Springer, New York. https://doi.org/10.1007/3-540-26468-x_1

Pulinets S (2004) Ionospheric precursors of earthquakes: recent advances in theory and practical applications. Terrestrial Atmos Oceanic Sci 15(3):413–435. https://doi.org/10.3319/TAO.2004.15.3.413(EP)

Randall AW, David HH (1993) Destructive upper-crustal earthquakes of Central America since 1900. Bull Seismol Soc Am 83(4):1115–1142. https://doi.org/10.1785/BSSA0830041115

Roy S, Bhunia GS, Shit PK (2020) Spatial prediction of COVID-19 epidemic using ARIMA techniques in India. Model Earth Syst Environ 7(2):1385–1391. https://doi.org/10.1007/s40808-020-00890-y

Schaffer AL, Dobbins TA, Pearson SA (2021) Interrupted time series analysis using autoregressive integrated moving average (ARIMA) models: a guide for evaluating large-scale health interventions. BMC Med Res Methodol 21(1):1–12. https://doi.org/10.1186/s12874-021-01235-8

Schekotov A, Hayakawa M, Potirakis SM (2021) Does air ionization by radon cause low-frequency atmospheric electromagnetic earthquake precursors? Nat Hazards 0123456789. https://doi.org/10.1007/s11069-020-04487-7

Schunk RW, Nagy AF (2010) Ionospheres. Physics, Plasma physics, and chemistry. CUP, Cambridge.

Şen Z (1992) Standard cumulative semivariograms of stationary stochastic processes and regional correlation. Math Geol 24(4):417–435. https://doi.org/10.1007/BF00891272

Şen Z (2016) Spatial modeling principles in earth sciences. Springer, Heidelberg. https://doi.org/10.1007/978-3-319-41758-5.pdf

Şen Z (2019) Earth systems data processing and visualization using MATLAB. Springer, Heidelberg. https://doi.org/10.1007/978-3-030-01542-8

Şen Z (2009) Spatial modeling principles in earth sciences. In Zekai S¸en(Istambul technical university) (Ed.), *Spatial modeling principles in earth sciences*. Springer US, New York, https://doi.org/10.1007/978-1-4020-9672-3

Şentürk E, Çepni MS (2018) 2016 Yılı 6 Mw ≥ 7.0 Depremin İyonküre Değişimlerinin İncelenmesi. Geomatik 3(1):35–47. https://doi.org/10.29128/geomatik.331208

Sevüktekin M, Çınar M (2017) Ekonometrik Zaman Serisi Analizi EViews Uygulamalı (5. Baskı, pp. 147–311). DORA Basım-Yayın Dağıtım. Bursa.

Sezen U, Arikan F, Arikan O, Ugurlu O, Sadeghimorad A (2013) Online, automatic, near-real time estimation of GPS-TEC: IONOLAB-TEC. Space Weather 11(5):297–305. https://doi.org/10.1002/swe.20054

Shah M, Jin S (2018) Pre-seismic ionospheric anomalies of the 2013 $M_w = 7.7$ Pakistan earthquake from GPS and COSMIC observations. Geodesy Geodyn 9(5):378–387. https://doi.org/10.1016/j.geog.2017.11.008

Sharma G, Champati Ray PK, Mohanty S, Kannaujiya S (2017) Ionospheric TEC modelling for earthquakes precursors from GNSS data. Quat Int 462:65–74. https://doi.org/10.1016/j.quaint.2017.05.007

Shumway RH, Stoffer DS (2017) ARIMA models, 4th edn. Springer, Cham, pp. 75–163. https://doi.org/10.1007/978-3-319-52452-8_3

Singh M, Kumar M, Jain RK, Chatrath RP (1999) Radon in ground water related to seismic events. Radiat Meas 30(4):465–469. https://doi.org/10.1016/S1350-4487(99)00049-9

Tanner AB (1964) Radon migration in the ground: a review. In: Adams JAS, Lowder WM (eds) Proceeding of the Natural Radiation Environment, Chap. 9, pp 161–190.

Tortum A, Gözcü O, Çodur MY (2014) Türkiye'de hava ulaşım talebinin arıma modelleri ile tahmin edilmesi. Iğdır Üniversitesi Fen Bilimleri Enstitüsü Dergisi 4(2):39–54

Ulomov VI, Mavashev BZ (1971) The Tashkent earthquake of 26 April, 1966. Acad. Nauk. Uzbek SSR FAN, 188–192.

Ulukavak M, Yalçınkaya M (2017a) Investigatıon of The Relationship Between Ionospheric TEC Anomaly Variatıons and Fault Types Before The Earthquakes. ISPRS Annals of Photogrammetry, Remote Sensing and Spatial Information Sciences, IV-4/W4, 383–388. https://doi.org/10.5194/isprs-annals-IV-4-W4-383-2017

Ulukavak M, Yalcinkaya M (2017b) Precursor analysis of ionospheric GPS-TEC variations before the 2010 M7.2 Baja California earthquake. Geomatics Nat Hazards Risk 8(2):295–308. https://doi.org/10.1080/19475705.2016.1208684

Wang X, Li Y, Du J, Zhou X (2014) Correlations between radon in soil gas and the activity of seismogenic faults in the Tangshan area, North China. Radiat Meas 60:8–14. https://doi.org/10.1016/j.radmeas.2013.11.001

Woith H (2015) Radon earthquake precursor: a short review. Euro Phys J Spec Topics 224(4):611–627. https://doi.org/10.1140/epjst/e2015-02395-9

Yaffee R, McGee M (1996) An introduction to time series analysis and forecasting, 1t edn, pp. 69–149. Academic Press, New York.

Yalım A, Sandıkçıoğlu A, Ertuğrul O, Yıldız A (2012) Determination of the relationship between radon anomalies and earthquakes in well waters on the Akşehir-Simav Fault System in Afyonkarahisar province, Turkey. J Environ Radioactivity 110:7–12. https://doi.org/10.1016/j.jenvrad.2012.01.015

Zhang X, Zhang T, Young AA, Li X (2014) Applications and comparisons of four time series models in epidemiological surveillance data. PLoS ONE 9(2):88075. https://doi.org/10.1371/journal.pone.0088075

Zhao XD, Du AM, Xu WY, Hong MH, Liu LB, Wei Y, Wang CG (2008) The origin of the prenoon-postnoon asymmetry for Sq current system. Acta Geophys Sinica 51(3):643–649. https://doi.org/10.1002/cjg2.1236

Zolotov OV, Namgaladze AA, Zakharenkova IE, Martynenko OV, Shagimuratov II (2012) Physical interpretation and mathematical simulation of ionospheric precursors of earthquakes at midlatitudes. Geomagn Aeron 52(3):390–397. https://doi.org/10.1134/S0016793212030152

Authors and Affiliations

Sinan Keskin[1] · **Fatih Külahcı**[1]

✉ Fatih Külahcı
fatihkulahci@firat.edu.tr

[1] Department of Physics, Nuclear Physics Division, Science Faculty, Firat University, 23100 Harput, Elazıg, Turkey